

# On the origin of the type-III radiation observed near the Sun

F.S. Mozer<sup>1,2</sup>, O. Agapitov<sup>1</sup>, S.D. Bale<sup>1,2</sup>, K. Goetz<sup>3</sup>,  
V. Krasnoselskikh<sup>4</sup>, M. Pulupa<sup>1</sup>, K. Sauer<sup>5</sup>, and A. Voshchepynets<sup>6</sup>

<sup>1</sup> Space Sciences Laboratory, University of California, Berkeley, California

<sup>2</sup> Physics Department, University of California, Berkeley, California

<sup>3</sup> University of Minnesota, Minneapolis, Minnesota

<sup>4</sup> LPC2E, CNRS-University of Orléans-CNES, 45071, Orléans, France

<sup>5</sup> Max-Planck Institute of Solar System Research, Göttingen, Germany

<sup>6</sup> Uzhhorod National University, Uzhhorod, Ukraine

## ABSTRACT

### *Aims.*

To investigate processes associated with generation of type-III radiation.

### *Methods.*

Measure the amplitudes and phase velocities of Parker Solar Probe observed electric fields, magnetic fields, and plasma density fluctuations.

### *Results.*

1. There are slow electrostatic waves near the Langmuir frequency and at as many as six harmonics. Their wave number is estimated to be 0.14 and  $k\lambda_d = 0.4$ . Even with a large uncertainty in this quantity (more than a factor of two) the phase velocity of the Langmuir wave was  $<10,000$  km/sec.

2. There is an electromagnetic wave near the Langmuir frequency having a phase velocity less than 50,000 km/sec.

3. Whether there are electromagnetic waves at the harmonics of the Langmuir frequency cannot be determined because the amplitudes of their magnetic fields would be below the instrument threshold.

4. The less-than-one-millisecond amplitude variations typical of the Langmuir wave and its harmonics are artifacts resulting from addition of two waves, one of which has small frequency variations that arise from propagation through density irregularities.

None of these results are expected in the conventional model of the three-wave interaction of two counter-streaming Langmuir waves that coalesce to produce the type-III wave. They are consistent with a new model in which electrostatic antenna waves are produced at the harmonics by radiation of the Langmuir wave, after which at least the first harmonic wave evolved through density irregularities until its wave number decreased and it became the type-III electromagnetic radiation.

## Introduction

An important wave near the Sun is the Type-III radiation, which is an electromagnetic wave whose frequency decreases with time and distance from the Sun. The theory of type-III bursts was described by Ginsburg and Zhelezniakov [1958] as a multi-step process in which Langmuir waves are produced by an electron beam, after which some of these waves interact with density irregularities to become backward waves that coalesce with the forward waves in a three-wave process that produces the electromagnetic type-III radiation. The theory has subsequently been discussed and refined by many authors (e.g. Sturrock 1964; Zheleznyakov & Zaitsev 1970; Smith 1970; Smith et al. 1976; Melrose 1980c; Goldman 1983; Dulk 1985; Melrose 1987). The first in-situ spectral observations of plasma waves in association with type-III emissions were made by Gurnett and Anderson [1976]. Their simultaneous observation of Langmuir waves, harmonic electric field emissions, and electromagnetic waves

was presented as evidence of the direct conversion of pairs of Langmuir waves into type-III waves, although the direct, in-situ, evidence of this interaction was not and has not been obtained.

## Data

On March 21, 2023, the Parker Solar Probe was located about 45 solar radii from the Sun when it became embedded in the active type-III emission region illustrated in Figure 1a. Note the colored lines under the emission (at the plasma frequency) which indicate times when large electric fields appeared. The type-III emission covered the frequency range from about 200 to 400 kHz at the time of about 26 bursts of high-rate data illustrated in Figure 1b. These bursts each consisted of  $\sim 15$  milliseconds of electric and magnetic field measurements at a data rate of about 1.9 million samples/second [Bale et al, 2016]. That the emission range covered more than just twice the plasma frequency has

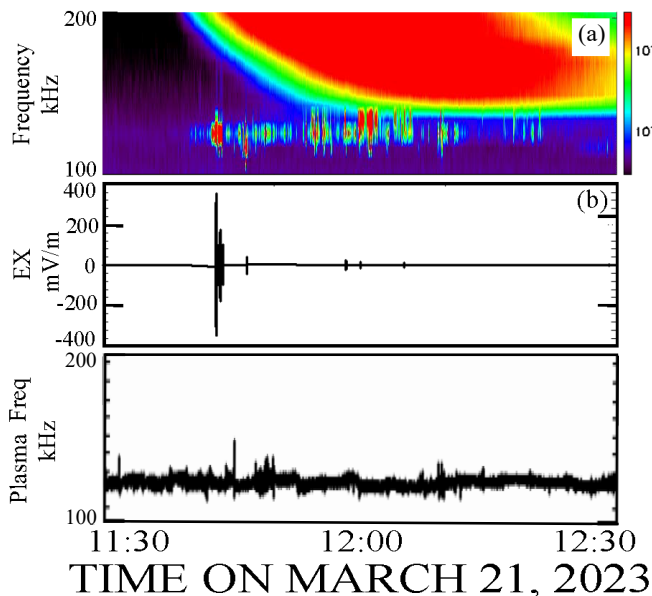


**Fig. 1.** Overview of a type-III emission observed on March 21, 2023 (panel 1a) in which the spacecraft was embedded, showing bright lines below the emission due to large electric fields. From the plasma frequency of 125 kHz in Figure 1c, it is seen that these bright lines were due to waves at or near the plasma frequency. Note that these waves are present only part of the time. Figure 1b shows the times and electric field amplitudes of 26 data bursts taken for duration's of about 15 milliseconds each at data rates in excess of one million samples/second.

been noted earlier [Kellogg, 1980; Reiner and MacDowell, 2019; Jebaraj et al, 2023] and this aspect of the emission will be investigated below.

The local plasma frequency, illustrated in Figure 1c, was determined as  $8980N^{0.5}$ , where  $N$  is the plasma density obtained from a least-squares fit of the spacecraft potential to the square root of the density obtained from the quasi-thermal noise measurement [Pedersen et al. 1984; Mozer et al, 2022]. The relationship between the spacecraft potential and the plasma density results from the spacecraft potential being determined by equating the flux of photo-electrons that overcome the potential (to escape to infinity) with the incoming flux due to the random thermal electron current. Comparison of the frequency of Figure 1c with the vertical lines beneath the type-III emission in Figure 1a shows that the waves observed in the bursts were at or near the local plasma frequency.

To interpret these observations in more detail, eleven short bursts of data obtained during a 250 msec interval during the type-III emission are illustrated in Figures 2a through 2d. Panels 2a and 2b give the two electric field components in the spacecraft X-Y plane, which is the plane perpendicular to the Sun-satellite line. Figure 2c plots the density fluctuations,  $\Delta N/N$ . Figure 2d presents the angle between the Langmuir  $k$ -vector and the magnetic field in the X-Y plane. Because  $B_z$  was almost zero at this time, the error associated with ignoring the out-of-the-X-Y-plane components in this measurement is small. It shows that the waves were oblique to the magnetic field much of the time. The largest event in Figure 2, near 11:43:15.460 had a maximum electric field of 300 mV/m and is discussed in the following sections.

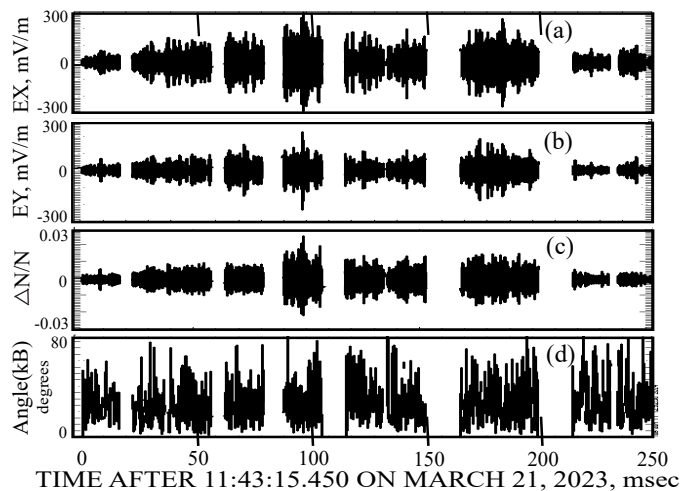


**Fig. 2.** Eleven short bursts of data obtained during a 250 msec interval during the type-III emission. Figures 2a and 2b give the X and Y components of the electric field in the spacecraft frame. Figure 2c gives the density fluctuations that are expected to accompany Langmuir waves. Figure 2d presents the angle in the X-Y plane between the background magnetic field and the electric field wave vector. The largest event, near 11:43:15.460 is discussed in the main text and the small and medium size events near 11:43:15.450 and 11:43:15.580 are discussed in the appendix.

The small and medium size events near 11:43:15.450 and 11:43:15.580 are discussed in the appendix.

In a Langmuir wave, the relationship between the density fluctuations and the electric potential is given as [Bellan, 2006]

$$\frac{\Delta N}{N} = \frac{e\phi}{m_e\omega_p^2/k_p^2} \quad (1)$$

where  $\phi$  is the potential of the wave,  $k_p$  is the wave number of the wave, and  $\omega_p = 2\pi \times 125$  kHz is the Langmuir wave frequency. This relationship is a direct consequence of the momentum equation and mass conservation law for electrons. This is the first measurement of the relationship between the density fluctuations and the wave potential although it has been studied previously [Neugebauer, 1975; Kellogg et al, 1999].

Figure 3a shows the electron velocity distribution function (vdf) during an 80 second interval surrounding the 15-millisecond large field event of Figure 2, using data obtained from on-board electron measurements [Whittlesey et al, 2020]. Because this data collection interval is about 5000 times greater than the duration of Figure 2 and because Langmuir waves appeared only a small fraction of this time (see Figure 1a), the vdf of Figure 3a is an average over an interval that is largely devoid of Langmuir waves. The currents obtained from the core and strahl distributions are 4.3 and -7.7 microamps/m<sup>2</sup>.

Figure 3b presents the hodogram of the electric field in the X-Y plane. Because, as noted,  $B_z \approx 0$ , the hodogram illustrates the relationship between the electric field  $k$ -vector and the magnetic field (the green line in Figure 3b). From 3b it is seen that the electric field was generally parallel to the background magnetic field with deviations that are described in Figure 2d.

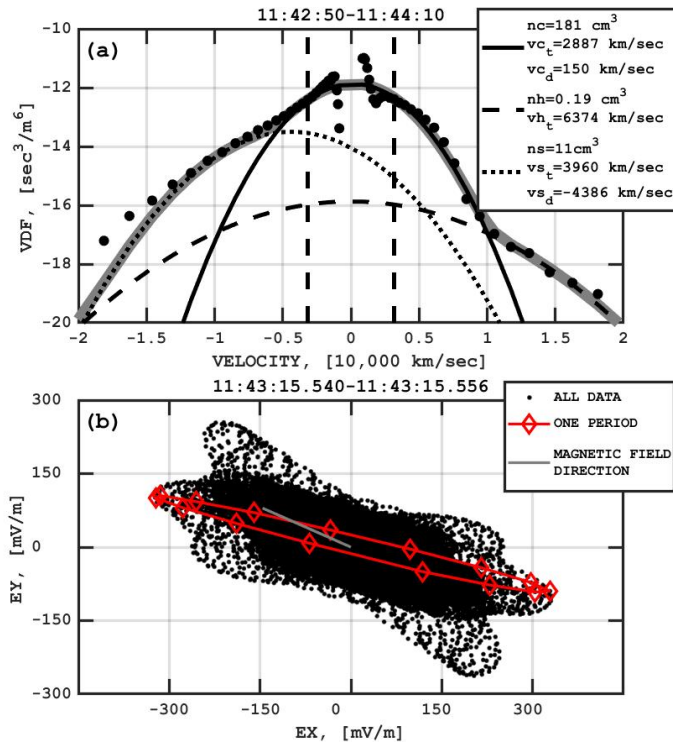


**Fig. 3.** Panel 3a gives the electron velocity distribution function during an 80 second interval surrounding the 15-millisecond large Langmuir wave. It describes the core, halo and strahl distributions which show that the average core electron density and thermal velocity were  $181 \text{ cm}^{-3}$  and  $2887 \text{ km/sec}$ . Panel 3b gives the hodogram of the electric field during this event. The hodogram is in the X-Y plane but, because  $B_z \approx 0$ , it describes the relationship between the electric field and the magnetic field direction, which is the green line. It is seen that the electric field is generally parallel to the magnetic field with significant deviations that are described in Figure 2d. The red curve in Figure 3b represents one period of the wave at the time of the data in Figure 5.

Figure 4 presents spectra of the electric field (black), magnetic field (red) and density fluctuations (green) for the largest event in Figure 2. (Similar results for both a small and a medium amplitude event are presented in the appendix). All three quantities in Figure 4 had spectral peaks near the plasma frequency of  $125 \text{ kHz}$ , with the magnetic field peak previously presumed to result from interaction of the plasma oscillations with ion sound waves to produce Z-mode waves [Gurnett and Anderson, 1976; Hospodarsky and Gurnett, 1995]. At the seven harmonics of the Langmuir frequency, prominent electric fields were observed having no measurable magnetic field components. If magnetic fields with amplitudes relative to that at the Langmuir frequency existed, they would be below the noise threshold of the measurement. That these harmonics are real and not artifacts of an imperfect measurement, is clear from the fact that, if they were not real, there would be no harmonics and no type-III emission. It is noted that other examples of wave spectra are given in Figures A1 and A2.

That the electric field instrument is capable of measurements at the frequencies observed in Figure 4 is verified from the fact that the time required to change the spacecraft potential by 1 volt through charging its  $1 \times 10^{-10}$  farad capacitance

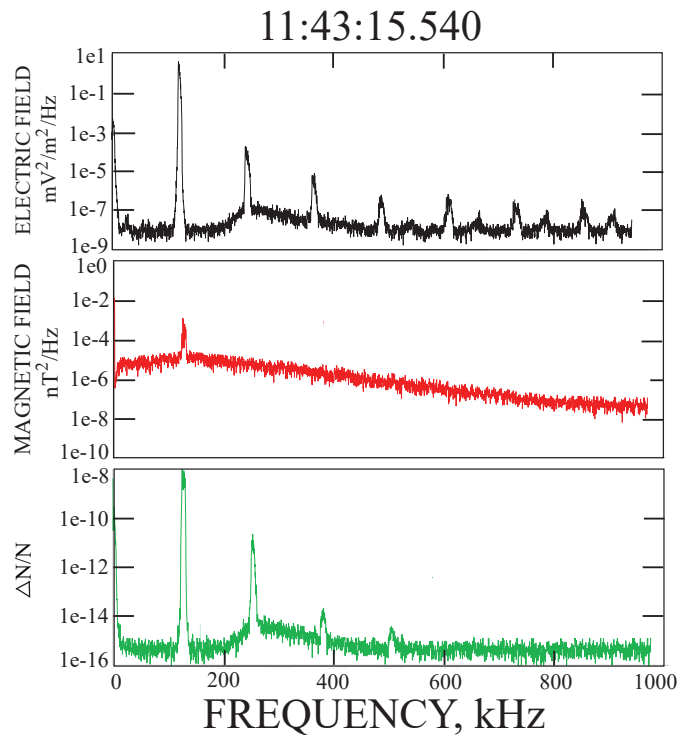


**Fig. 4.** Spectra of the electric field, the magnetic field and the density fluctuations observed during the intense burst of Figure 2. The lowest frequency wave, at  $125 \text{ kHz}$ , is at the Langmuir frequency and it has both a magnetic and density fluctuation component. Six electric field harmonics of the intense burst are observed and three of them have detectable density fluctuations.

by the photoemission current of about  $5 \times 10^{-3}$  amps is about  $2 \times 10^{-8}$  seconds.

Theories of such harmonic waves, produced in density cavities [Ergun et al, 2008; Malaspina et al, 2012], do not apply to the present observations because density cavities were not present at times of any of the events discussed on the day of interest. Instead, the harmonics were likely created by a single wave in an electron beam that grew exponentially until the beam electrons were trapped. At that time, the wave amplitude stopped growing and began to oscillate about a mean value. During the trapping process, the beam electrons were bunched in space and higher harmonics of the electric field were produced [O’Neil et al, 1971, 1972].

Properties of the electromagnetic waves near the Langmuir frequency may be obtained by considering the ratio of their electric fields to their magnetic fields, which, for a full field measurement, gives the phase velocity of the wave. Although only two components of E and one component of B were measured, their ratio can give an estimate of the phase velocity. In Figure 5, this ratio is plotted for the 11 events in Figure 2, and the average velocity thereby obtained is about  $50,000 \text{ km/sec}$ . This is an overestimate of the velocity because part of the electric field was in the electrostatic, not the electromagnetic, wave. With a frequency of  $125 \text{ kHz}$ , this wave had a wavelength that was less than 400 meters and a  $k$ -value greater than  $0.015$ . From the electron core temperature of  $23 \text{ eV}$  and the plasma density of  $181 \text{ cm}^{-3}$ , both obtained from the vdf of Figure 3a, the Debye length was  $2.65$  meters. Thus,  $k\lambda_d$  was greater than  $0.04$ .

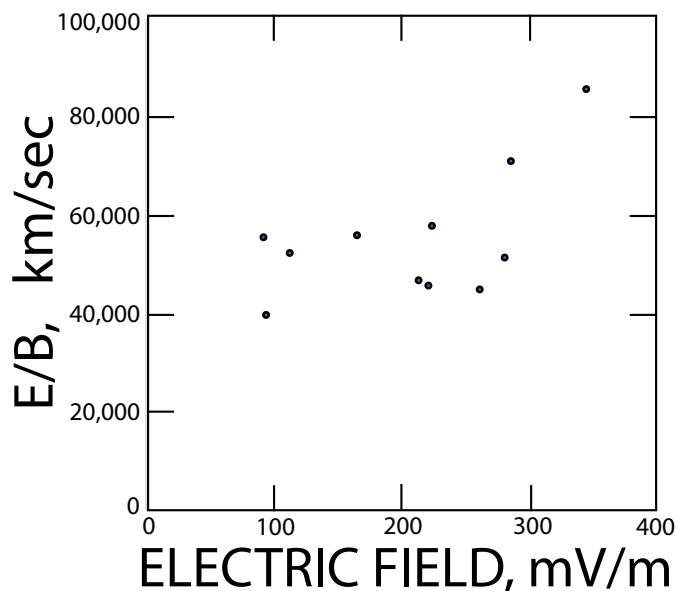


**Fig. 5.** A plot of a single component of the electric field divided by a single component of the magnetic field for the eleven events depicted in Figure 2. For a full measurement, this ratio is equal to the phase velocity of the wave. The ratio is an overestimate of the phase velocity of the electromagnetic wave because part of the electric field resulted from an electrostatic wave. Thus, the phase velocity of the electromagnetic wave was  $<50,000$  km/sec.

The phase velocity of the Langmuir wave may be estimated from equation (1), using the measured electric field of 250 mV/m and density fluctuations of 0.02 in Figure 2. With uncertainties in each of these quantities of about a factor of two, the  $k$ -value obtained from equation (1) is 0.14. This gives  $k\lambda_d = 0.4$  and a phase velocity of the electrostatic wave that was less than 10,000 km/sec.

When a positive electric field in the wave passes over the spacecraft,  $V1$  (which is the potential of antenna 1 minus the spacecraft potential), first becomes positive and then,  $V2$  becomes negative (because the spacecraft potential becomes positive before the antenna potential becomes positive). Their time difference gives the time required for the wave to propagate across the antenna system, which is proportional to the phase velocity of the wave. While the phase velocity of the electrostatic wave can be estimated in this way, in fact this time difference actually varied over a range so wide that such a measurement was not possible. In addition, the ratio of the few volt amplitude of  $V1$  to the amplitude of  $V2$  varied by almost two orders-of-magnitude, as illustrated in Figure 6a. These facts must be due to the presence of two waves whose amplitudes at each antenna add together to produce the observed wave. However, two waves with constant and different frequencies add to produce beats like those in Figure 6c, and this is not what is observed. Because the Langmuir wave frequency is proportional to the square root of the density, its frequency varied with time as it passed over density irregularities. As seen from the density plot of Figure 6b, this is an important effect because the density varied by as much as 10 percent in the vicinity of the observations. Allowing the Langmuir wave frequency to vary pseudo-randomly by one or two percent would produce many different curves, a typical one of which is illustrated from a simulation in Figure 6d. Thus, it is

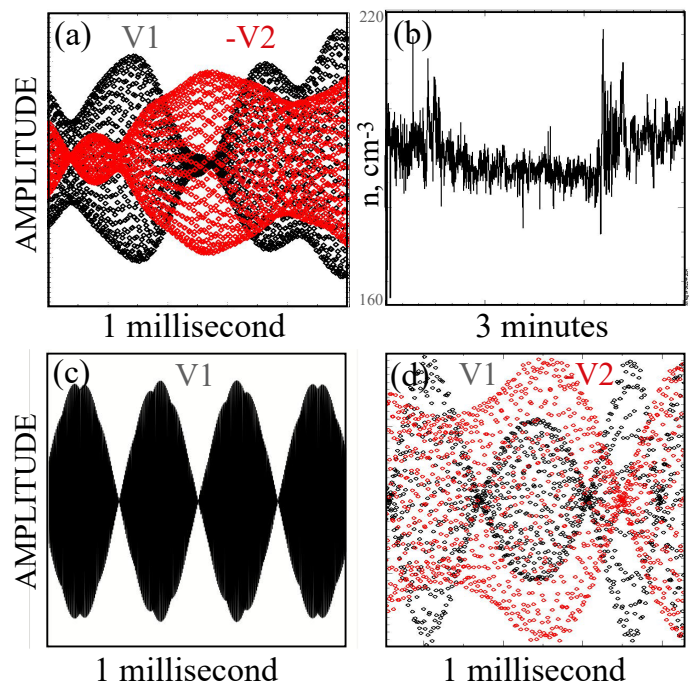


**Fig. 6.** Panel 6a gives the few volt potentials on antennas 1 and 2 during a one millisecond interval. Their difference must be due to the addition of two waves at each antenna, with the Langmuir wave having a variable frequency to avoid the beats produced by two fixed-frequency waves, as illustrated in panel 6c. The Langmuir wave frequency varied because of the large density irregularities illustrated in panel 6b, to produce a simulation in panel 6d of the signals on the two antennas that are produced by one or two percent Langmuir wave frequency variations.

concluded that the signal near the Langmuir frequency is made of an electromagnetic wave having a phase velocity of about 25,000 km/sec and a Langmuir wave whose frequency varied as it passed over density irregularities. As seen in appendix Figure A3, the harmonics of two other waves each also contained two waves, one of which had a frequency that also varied during its passage over the spacecraft because such variations of the voltage ratio and time delay also occurred in that data.

It is important to note that the rapid (less than one millisecond) amplitude variations typical of the Langmuir wave and its harmonics are artifacts resulting from addition of two waves, and that the observed wave amplitude is not representative of the true wave amplitude versus time.

## Discussion

The above analyses show that slow electrostatic waves (phase velocity  $< 10,000$  km/sec) existed near the Langmuir frequency and at as many as six harmonics, the number of which increases with the amplitude of the Langmuir wave. Their electrostatic nature is shown by measurements of density fluctuations of the appropriate magnitudes at each frequency. These harmonics were likely created by a single wave in an electron beam that grew exponentially until the beam electrons were trapped. At that time, the wave amplitude stopped growing and began to oscillate about a mean value. During the trapping process, the beam electrons were bunched in space and higher harmonics of the electric field were produced [O'Neil et al, 1971, 1972]. Conversion of these

harmonics to electromagnetic waves via propagation through an inhomogeneous plasma having density fluctuations is a process that has been well-studied [Stix, 1965; Oyo, 1971; Melrose, 1980a; Melrose, 1981; Mjølhus et al, 1983; Morgan and Gurnett, 1990; Kalaee et al, 2009; Schleyer et al, 2013; Kim et al, 2013; Kalaee et al, 2016]. It is plausible that the Langmuir frequency harmonics were converted to type-III emissions in this way.

It is emphasized that none of these results are required or explained by the conventional model of the three-wave interaction of two counter-streaming Langmuir waves that coalesce to produce the type-III wave. In fact, no evidence has been found in this or earlier studies that requires this coalescence model for its understanding.

There is also an electromagnetic wave near the Langmuir frequency having a phase velocity less than 50,000 km/sec. Whether there are electromagnetic waves at the harmonics of the Langmuir frequency cannot be determined because, if they existed, their magnetic field components would be below the noise level of the measurement. A possible explanation of this wave and the existence of a slow electrostatic wave is next given.

The following discussion of current-driven generation of electrostatic and electromagnetic fields at frequencies very close to the electron plasma frequency,  $\omega_p$ , is based on the results of previous studies [Sauer and Sydora, 2015, 2016; Sauer et al, 2017, 2019] on the excitation of current-driven Langmuir oscillations with  $\omega = \omega_e$  and  $k = 0$  by which, subsequently, a parametric decay in Langmuir and ion-acoustic waves with finite wave number is triggered. It is assumed that the electron component is composed of two parts: a dominant population at rest and a minor component in relative motion, as seen in the core, halo and strahl of Figure 3. The mechanism of wave excitation does not take into account beam instabilities that may occur in an earlier phase of the interaction. The electron current resulting from the relative motion between the two electron components is crucial for triggering the Langmuir oscillations.

A characteristic electron velocity distribution function of the solar wind is shown in Figure 7a together with the related dispersion of Langmuir waves in the wave number range up to  $k\lambda_d = 0.6$ . As seen in Figure 7b, due to the occurrence of the electron-acoustic mode which is associated with the strahl, mode splitting takes place at the point where the Langmuir mode of the main population is crossed, that is at  $k\lambda_d \approx 0.3$ . Correspondingly, the related phase velocity is  $V_{ph} \approx 3.5V_e$  (Figure 6b). Around this point the Langmuir/electron-acoustic mode is weakly damped (Figure 7c) and its frequency approaches the plasma frequency,  $\omega_p$ , (see red points). As shown in earlier papers [Sauer and Sydora, 2015, 2016, Sauer et al, 2017, 2019], the current due to the strahl drives Langmuir oscillations at  $\omega_e$  and simultaneously Langmuir/electron-acoustic waves are driven by parametric decay. Their wave length is given by that of the electron-acoustic mode at  $\omega \approx \omega_e$ , which in the present case is  $k\lambda_d \approx 0.3$ .

Four arguments supporting the validity of the observed density data are:

1. In other publications, density fluctuations obtained from the spacecraft potential have been observed and shown

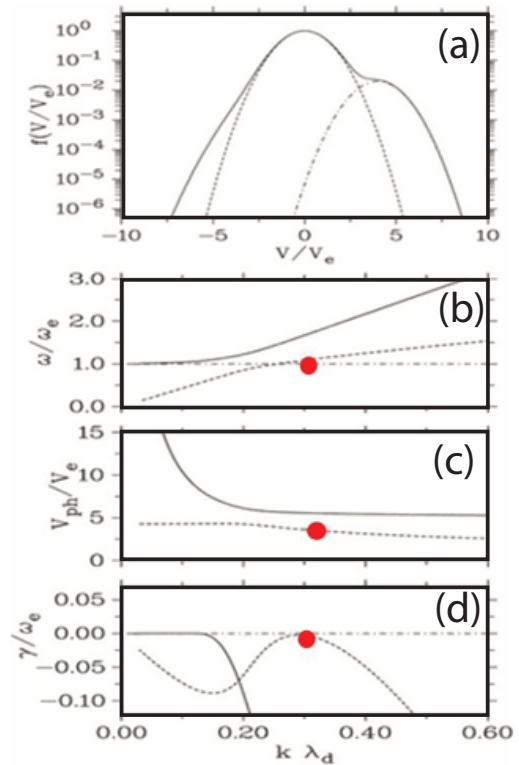


**Fig. 7.** a) Model electron velocity distribution function (EVDF) of the solar wind consisting of core, halo and strahl and the associated dispersion of the Langmuir/electron-acoustic mode. b) frequency  $\omega/\omega_e$ , c) phase velocity  $V_{ph}/V_e$ , where  $V_e$  is the thermal core velocity, and d) damping rate  $\gamma/\omega_e$ .

to be valid at low and high frequencies [Roberts et al, 2020; Mozer et al, 2023]. Such fluctuations have also been observed in laboratory measurements [Hu, 2021].

2. Figure 1c illustrates the Langmuir frequency obtained from the plasma density which, in turn, was obtained from the spacecraft potential. That the plasma frequency of Figure 1c agrees with the measured plasma frequency of Figure 1a is proof of the validity of the low frequency density estimate obtained from the spacecraft potential.
3. Equation (1) presents the theoretical relationship between the electric potential (or field) in the wave and the density fluctuations,  $\Delta N/N$ , that is required in an electrostatic wave. That the ratio of the electric field to  $\Delta N/N$  in this equation is within a factor of two equal to the more variable measured ratios, is evidence that determination of the density from the spacecraft potential is valid at high frequency.
4. A further requirement of equation (1) is that the electric field and density fluctuation in the high frequency wave be 90 degrees out of phase. This has been found to be the case (see Figure A4 in the appendix) which provides conclusive evidence that the electric field and  $\Delta N/N$  were well-measured and that they were not artifacts of a poor measurement.

Previously observed Langmuir wave electric fields have ranged from a few to about 100 mV/m [Gurnett and Anderson, 1976; Graham and Cairns, 2012; Sauer et al, 2017]. This range is associated with the range of driving current densities in the plasma. The observed electric field of about 300 mV/m is a factor of three larger than the largest of the

previously observed Langmuir waves [Malaspina et al 2010]. The explanation of this difference may lay in the fact that the Langmuir waves had a wavelength that was longer than the three-meter Parker Solar Probe antenna but was similar to or shorter than the typical antennas that made the earlier measurements. An antenna that is longer than the wavelength of the wave, under-estimates the amplitude of the true electric field because of the many wavelengths of the field that are inside the antenna. This antenna property may explain why the largest earlier electric field measurements were smaller than observed in the current example.

The rapid (less than one millisecond) amplitude variations typical of the Langmuir wave and its harmonics are artifacts resulting from addition of two waves, one of which has small frequency variations that arise from traveling through density irregularities.

## Acknowledgements

This work was supported by NASA contract NNN06AA01C. The authors acknowledge the extraordinary contributions of the Parker Solar Probe spacecraft engineering team at the Applied Physics Laboratory at Johns Hopkins University. The FIELDS experiment on the Parker Solar Probe was designed and developed under NASA contract NNN06AA01C. Our sincere thanks to J.W. Bonnell, M. Moncuquet, and P. Harvey for providing data analysis material and for managing the spacecraft commanding and data processing, which have become heavy loads thanks to the complexity of the instruments and the orbit.

## References

- Bale, S. D., Burgess, D., Kellogg, P. J., Goetz, K., Howard, R. L., & Monson, S. J., 1996. *GRL*, **23**, 109–112. <https://doi.org/10.1029/95GL03595>
- Bale, S.D., Kellogg, P.J., Goetz, K., and Monson, S.J., 1998, *GRL*, **25**, NO. 1, 9-12
- Bale, S. D., Goetz, K., Harvey, P. R., et al. 2016, *SSRv*, **204**, 49
- Bellan, P.M. 2006, Cambridge University Press, <https://doi.org/10.1017/CBO9780511807183>
- Dulk, G. A. 1985, *ARA&A*, **23**, 169
- Ergun, R.E., Malaspina, D.M., Cairns, I.H, et al, 2008, *PRL* **101**
- Ginzburg, V.L. and Zheleznyakov, V.V., *Sov. Astron. AJ* **2**, 653 (1958)
- Goldman, M. V., Reiter, G.F. and Nicholson, D.R., 1980, *Phys. Fluids*, **23**, 388 – 401.
- Graham, B., and Cairns, I.H., 2012, *JGR: SPACE PHYSICS*, **118**, 3968–3984, doi:10.1002/jgra.50402
- Gurnett, D. A. and Anderson, R. R. 1976. *Science*. **194** (4270): 1159–1162
- Henri, P., Briand, C., Mangeney, A., Bale, S. D., Califano, F., Goetz, K., & Kaiser, M., 2009, *JGR*, **114**(A13), 3103. <https://doi.org/10.1029/2008JA013738>
- Hospodarsky, G.B. and Gurnett, D.A., 1995, *GRL*, **22**, NO. 10, 1161-1164
- Hu, Y., Yoo, J., Ji, H., Goodman, A., and Wu, X. ,2021, *Rev. Sci. Instrum.* **92**, 033534; doi: 10.1063/5.0035135
- Jebaraj,I.C., Krasnosalskikh, V., Pulupa, M., Magdalenic, J., and Bale, S.D. , 2023, *Ap.J.*, **955:L20** <https://doi.org/10.3847/2041-8213/acf85>
- Kalae, M.J., Ono, T. Katoh, Y, Lizima, M., and Nishimura, Y., 2009, *Earth Planets Space*, **61**, 1243–1254
- Kalae, M.J., Katoh, Y., 2016, *Phys. Plasmas*, **23**, 072119, <https://doi.org/10.1063/1.4958945>
- Kellogg, P.J., 1980, *Ap.J.*, **236**, 696-700
- Kellogg, P.J., Goetz, K, and Monson, S.J., 1999, *JGR*, **104**, A8, 17,069-17,078
- Kim, E.H., Cairns, I.H. and Johnson, J.R., 2013, *Phys. Plasmas*, **20**, 122103
- Larosa, A., Dudok de Wit, T., Krasnoselskikh1, V., Bale, S.D., Agapitov, O., Bonnell, J.W., et al, 2022, *Ap.J.*, 927:95 (8pp) <https://doi.org/10.3847/1538-4357/ac4e85>
- Malaspina, D.M., Cairns, I.H., and Ergun, R.E. 2010, *JGR*, **115**, A01101, doi:10.1029/2009JA014609
- Malaspina, D.M., Cairns, I.H., and Ergun, R.E. 2012, *Ap.J.*, **755:45**, doi:10.1088/0004-637X/755/1/45
- Malaspina, D. M., Graham, D.B., Ergun, R.E.,and Cairns, I.H., 2013, *JGR, Space Physics*, **118**, 6880–6888, doi:10.1002/2013JA019309
- Melrose, D. B. 1980, *Space Sci. Rev.*, **26**, 3
- Melrose, D.B., 1980a, *Aust. J. Phys*, **33**,661
- Melrose, D.B., 1981, *Journal of Geophysical Research: Space Physics*, **86**, Issue A1 / p. 30-36, <https://doi.org/10.1029/JA086iA01p00030>
- Melrose, D. B. 1987, *Sol. Phys.*, **111**, 89
- Mjølhus, E., 1983, *Journal of Plasma Phy*, **30** Issue 2 pp. 179 - 192 DOI: <https://doi.org/10.1017/S0022377800001>
- Morgan, D.D., and Gurnett, D.A., 1990, *Radio Sci.*,**25**(6), 1321–1339, doi:<https://doi.org/10.1029/RS025i006p01321>
- Mozer, F.S., Bale, S.D., Kellogg, P.J., Larson, D., Livi, R., Romeo, O., 2022, *The Astrophysical Journal*, **926**, Issue 2, DOI:10.3847/1538-4357/ac4f42
- Mozer, F.S., Agapitov, O., Bale, S.D., Livi, R., Romeo, O., Sauer, K., Vasko, I.Y., Verniero, J., 2023, *ApJL*, **957** DOI 10.3847/2041-8213/ad0721
- Neugebauer, M., 1976, *Geophys. Res.*, **81**, 2447, 19
- O’Neil, T. M., Winfrey, J. H., Malmberg, J. H. ,1971, *Physics of Fluids*, **14**, 6, p.1204-1212 DOI:10.1063/1.1693587
- O’Neil, T. M., Winfrey, J. H., 1972, *Phys. Fluids* **15**, 1514–1522 (1972) <https://doi.org/10.1063/1.1694117>
- Oyo, H., 1971, *Radio Science*, **6**, Issue 12, pp. 1131-1141 DOI:10.1029/RS006i012p01131
- Papadopoulos, K., Freund, H.P. 1978, *Geophys. Res. Lett.*, **5**, 881 – 884

Pedersen, A., Cattell, C., Falthammar, C-G., Formisano, V., Lindqvist, P-A., Mozer, F., and Torbert, R., 1984, *Space Sci. Rev.* **37**, 269-312

Reiner, M.J. and MacDowall, R.J., 2019, *Solar Phys* (2019) 294:91 <https://doi.org/10.1007/s11207-019-1476-9>

Roberts, O.W., Nakamura, R., Torkar, K., Graham, D.B., Gershman, D.J., Holmes, J.C., et al. 2020, *J.G.R., Space Physics*, **125**, <https://doi.org/10.1029/2020JA02785>

Sauer, K., and Sydora, R., 2015, *JGR, Space Physics*, 120, doi:10.1002/2014JA020409.

Sauer, K., and Sydora, R., 2016, *Geophys. Res. Lett.*, 43, doi:10.1002/2016GL069872.

Sauer, K., Malaspina, D.M., Pulupa, M. and Salem, C.S., 2017, *J. Geophys. Res. Space Physics*, 122, 7005–7020, doi:10.1002/2017JA024258

Sauer, K., Baumgärtel, K., Sydora, R., and Winterhalter, D. 2019, *JGR, Space Physics*, 124, 68–89. <https://doi.org/10.1029/2018JA025887>

Schleyer, F., Cairns, I.H. and Kim, E.-H. 2013, *Phys. Plasmas* **20**, 032101, <https://doi.org/10.1063/1.4793726>

Smith, D. F. 1970, *Sol. Phys.*, 15, 202

Smith, R. A., Goldstein, M. L., and Papadopoulos, K. 1976, *Sol. Phys.*, 46, 515

Stix, T.H. ,1965, *Phys. Rev. Lett.*, **15**, 23

Sturrock, P. A. 1964, *NASA Special Publication*, 50, 357

Whittlesey, P.L., Berthomier, M., Larson, D.E., Case, A.W., Kasper, J.C., et al, 2020, *Ap.J.*, 246, <https://doi.org/10.3847/1538-4365/ab7370>

Zheleznyakov, V. V., & Zaitsev, V. V. 1970, *Soviet Ast.*, 14, 47

### Power spectra of a 30 mV/m Langmuir wave

In Figure A1, the spectra associated with a lower amplitude Langmuir wave are displayed. Although this wave was an order-of-magnitude smaller than the wave having the spectra of Figure 4, the peaks near the plasma frequency and its first harmonic of the electric field of panel A1(a), the magnetic field of panel A1(b) and the density fluctuations of panel A1(c) show that this wave and its harmonic were also slow electrostatic waves.

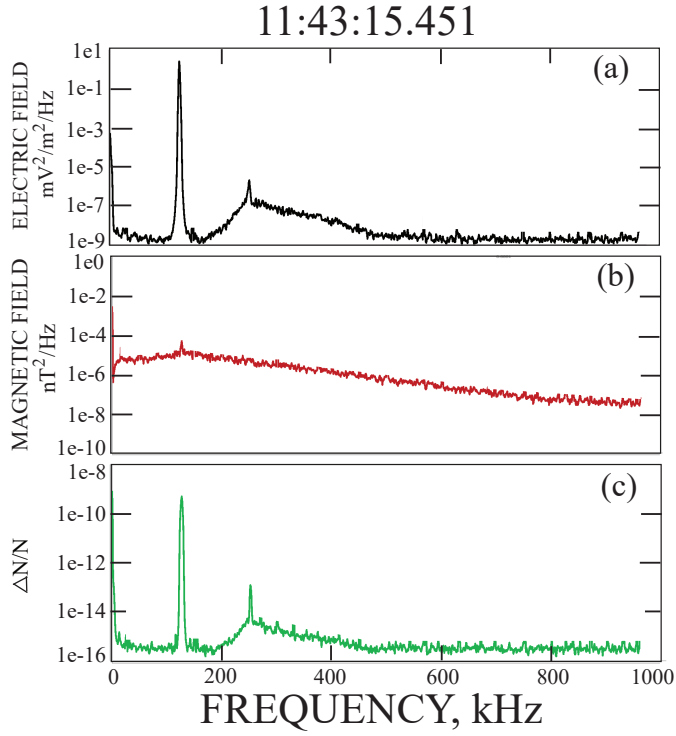


Fig. A1. Spectra of a 30 mV/m Langmuir wave.

### Power spectra of a 150 mV/m Langmuir wave

The wave of Figure A2 also shows spectral peaks similar to those observed for a 300 mV/m wave (Figure 4) and a 30 mV/m wave (Figure A1). These same peaks were observed for all waves in Figure 2, so they were typical of the waves observed during the type-III emission..

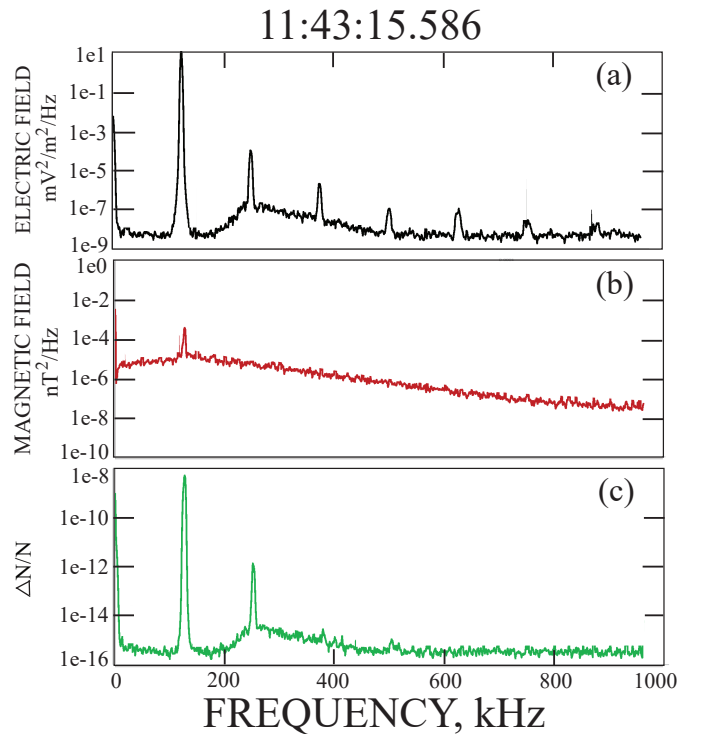


Fig. A2. Spectra of a 150 mV/m Langmuir wave

### Antenna potentials for plasma frequency and first harmonic waves observed at two different times

Figure A3 illustrates the single-ended potentials  $V1$  and  $-V2$  for the plasma waves of panels A3(a) and A3(b) and their first harmonics in panels A3(c) and A3(d) at the time of the low amplitude plasma waves in panels A3(b) and A3(d) and the medium amplitude plasma waves in panels A3(a) and A3(c). Because, in all cases, the ratio of the two potentials varied by large factors, pairs of electrostatic waves existed during both the events with at least one of the pair being slow. This same behavior was observed for all the bursts of Figure 2.

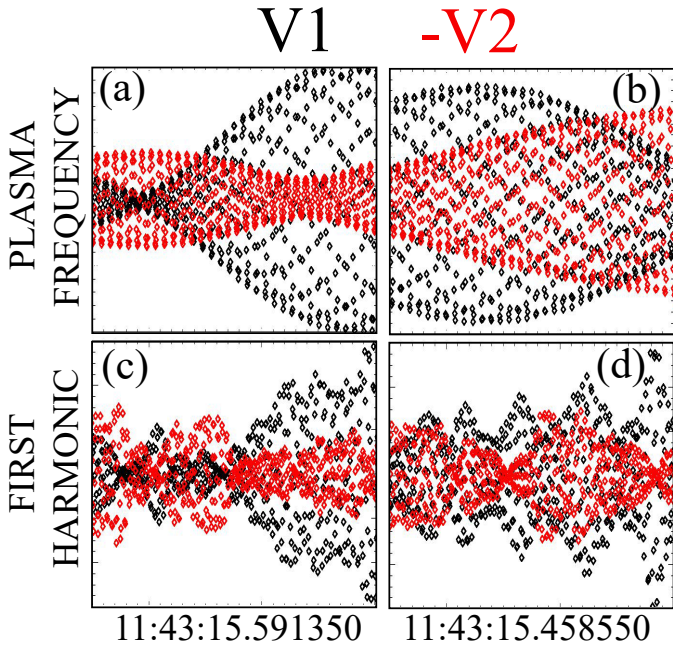


Fig. A3. Single-ended antenna potentials for two wave events.

### Relative timing of the electric field and the density fluctuations

Equation 1 requires that the electric field and density components of a wave be 90 degrees out of phase. This requirement is verified in Figure A4, which illustrates several cycles of the electric field and density fluctuations near the plasma frequency in panels A4(a) and A4(b) and the first harmonic in panels A4(c) and A4(d). For each case a vertical dashed line allows comparison of the phase difference between the E-field and the density wave, which is found to be close to 90 degrees. This result supports the conclusion that the waves were accurately measured.

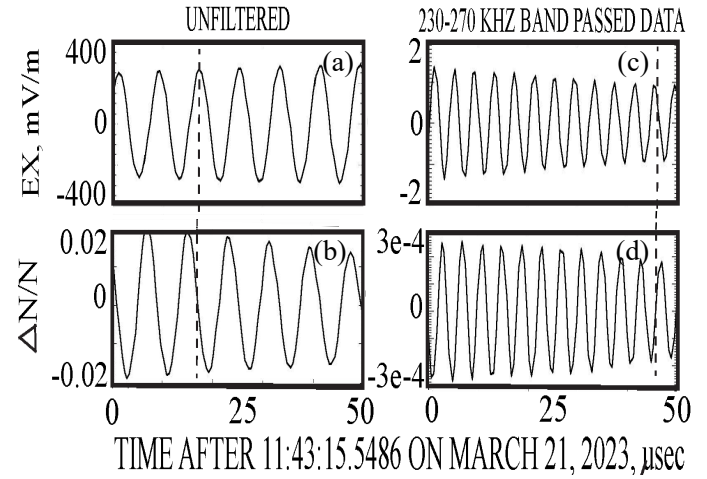


Fig. A4. Relative timing of the electric field and density waves.